

NeuroTrainer: An Intelligent Memory Module for Deep Learning Training

Duckhwan Kim¹, Taesik Na¹, Sudhakar Yalamanchili¹, and Saibal Mukhopadhyay¹

¹School of Electrical and Computer Engineering, Georgia Institute of Technology, Atlanta, GA 30332, USA

ABSTRACT

This paper presents, NeuroTrainer, an intelligent memory module with in-memory accelerators that forms the building block of a scalable architecture for energy efficient training for deep neural networks. The proposed architecture is based on integration of a homogeneous computing substrate composed of multiple processing engines in the logic layer of a 3D memory module. NeuroTrainer utilizes a programmable data flow based execution model to optimize memory mapping and data re-use during different phases of training operation. A programming model and supporting architecture utilizes the flexible data flow to efficiently accelerate training of various types of DNNs. The cycle level simulation and synthesized design in 15nm FinFET shows power efficiency of 500 GFLOPS/W, and almost similar throughput for a wide range of DNNs including convolutional, recurrent, multi-layer-perceptron, and mixed (CNN+RNN) networks.

1. INTRODUCTION

The hardware acceleration of *inference* of Deep Neural Network (DNNs) including convolutional (CNN), recurrent (RNN), and multi-layer-perceptron (MLP) have received considerable attention in recent past [1, 2, 3, 4, 5, 6, 7, 8, 9]. In contrast, training has largely been accelerated by software implementations executing on clusters of graphics processing units (GPUs). As DNNs become larger and more complex, the time and energy costs of training become limiters to the application of DNNs to more complex problems. For example, a DGX-1 with 8 GPUs consumes more than 3KW, and is limited to training only 1,000 Imagenet images per second for VGG 16 [10]. Hence, availability of a specialized modular architecture for energy efficient scaling of training performance will be critical to the feasibility of future, large scale DNNs.

The training of a DNN is composed of three primary steps: forward propagation (FP), which is identical to inference, back propagation (BP), and parameter update (UP) (see Section 2 for details). The acceleration of training faces major additional challenges over acceleration of inference as discussed below.

1) Most DNN accelerators for inference are optimized for convolutions with small kernels and matrix-matrix multiplication (for fully connected layers). However, accelerating BP and UP includes the following additional operations - i) convolution with very large kernels, ii) matrix transpose, iii) vector to vector outer product, iv) loss function computation, v) a pooling layer and its derivative, and vi) the derivative of non-linear activation functions..

2) Training operates over very large data sets and employs mini-batch processing across training thereby requiring larger on-chip storage to increase effective memory bandwidth. In contrast, inference operates over single sample. Further, while inference requires only reading weights, training requires reading/writing weights and their gradients, increasing memory traffic.

3) The computation of gradients in back propagation and weight update require higher bit precision to account for small gradient values (vanishing gradient issue [11, 12]). Therefore, low bit precision (8/16 bit) arithmetic, often used during inference for energy efficiency, is not suitable for training.

This paper presents, NeuroTrainer, an intelligent memory module with in-memory accelerators that forms the building block of a scalable architecture for energy efficient training. The key distinguishing feature of NeuroTrainer is its programmable data flow execution model. We observed that distinct computational kernels in training different networks share common arithmetic operations (e.g., multiply-and-accumulate) but differ in their memory usage and data flow pattern. Hence, NeuroTrainer utilizes a homogeneous architecture but with an execution model where memory mapping, re-use, and data flow for different kernels are programmed to match the data usage/flow pattern, and hence, optimize performance of each kernel. It is in contrast to recent report of multi-chip module based training accelerator where each chip is independently optimized for a specific operation, creating a heterogeneous architecture [13]. A major advantage of the programmable data-flow based execution on homogeneous substrate, compared to customized hardware based solutions is to provide stable performance over many applications.

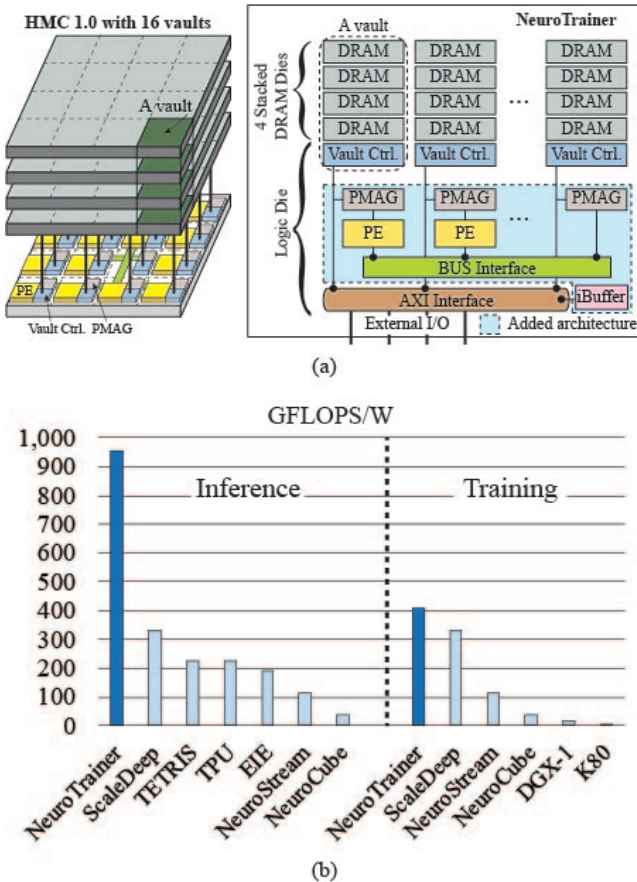


Figure 1: NeuroTrainer overview: (a) Proposed architecture. (b) Efficiency (GFLOPS/W)

The NeuroTrainer is evaluated using cycle level simulation, and synthesized in 15nm FinFET technology. The NeuroTrainer demonstrates 25x higher efficiency over GPU (Fig. 1). Moreover, NeuroTrainer shows higher average power efficiency over prior training accelerators [4, 6, 13], and more importantly, demonstrate ability to train different types of benchmark networks (CNN, RNN, and CNN + RNN) with similar power-efficiency. We further demonstrate scalable system with multiple interconnected NeuroTrainers to scale training performance for very large DNNs. Hence, NeuroTrainer can be used as the building block to design a large scale DNN training platform.

This paper makes the following contributions.

1) We present a programmable data flow based execution model that enables the use of a homogeneous computing architecture to efficiently train diverse DNNs. This flexible data flow programmability enables efficiently accelerate training of various types of DNNs including CNNs, RNNs, MLPs and hybrid networks (CNN+RNN).

2) We present the NeuroTrainer as a 3D memory module with an integrated in-memory accelerator. The architecture of the memory module is patterned after

the Hybrid Memory Cube (HMC) which is composed of stacked DRAM partitioned across multiple independently controlled *vaults*. Each vault has an independent vault controller on the logic die; therefore multiple partitions in a DRAM die can be accessed simultaneously.

3) We present an in-memory accelerator composed of an array of interconnected processing engines (PEs), implemented on the logic die with precision-configurable arithmetic and support for dataflow based execution. All but one memory vault are connected to a dedicated PE; and the remaining vault is connected to all the PEs using a shared bus. Each vault controller is augmented with a Programmable Memory Address Generator (PMAGs).

4) We develop programming model for the NeuroTrainer. Compilation now involves optimized mappings of data (input, parameters, and gradients) into memory vaults, and programming the PMAGs to orchestrate an efficient flow of data between the DRAM and logic layer in a manner that optimizes bandwidth, exploits re-use, maximizes concurrency, and minimizes data movement and buffering in the PEs.

The rest of the paper is organized as follows. Section 2 introduces DNN training; Section 3 illustrates the proposed architecture; Section 4 explains the programming model; Section 5 presents simulation results, followed by related work and conclusion.

2. PRELIMINARIES

In this section, we will explain the approach for training DNN with gradient descent, which is composed of three steps: feedforward, backpropagation, and weight update in recent DNNs [14]. Fig. 2 shows a simple DNN and its feedforward, backpropagation, and weight updating for different types of the layer in the network.

2.1 Feedforward (FF)

Feedforward is propagation of neuron activation from i^{th} layer to $i + 1^{th}$ layer through weights between two layers. The output of a neuron (state) is weighted summation of activation from all connected neurons in previous layer (and current layer as well for RNN [15]). It is the only phase required during the inference. Fig. 2 shows feedforward through convolution layer and fully connected layer.

2.2 Backpropagation (BP)

For a given input, at the end of feedforward operation, the output of the last layer is compared with the *ground truth* i.e. the desired output for this input and computing loss (L). The loss can be defined by simple mean squared error (MSE) or combination of softmax layer and cross-entropy layer [16]. Backpropagation is the phase to find the impact of each state on the loss (gradient) $\partial L / \partial X (dX)$ by propagating from the last layer. Since there is no definition of loss (L) in hidden layer, $\partial L / \partial X (dX)$ is computed from the dX of $i + 1^{th}$ layer ($\partial L / \partial Y (dY)$) instead of computing $\partial L / \partial X (dX)$ directly. We can see most of *arithmetic* operation in Backpropagation is similar to that of Feed-

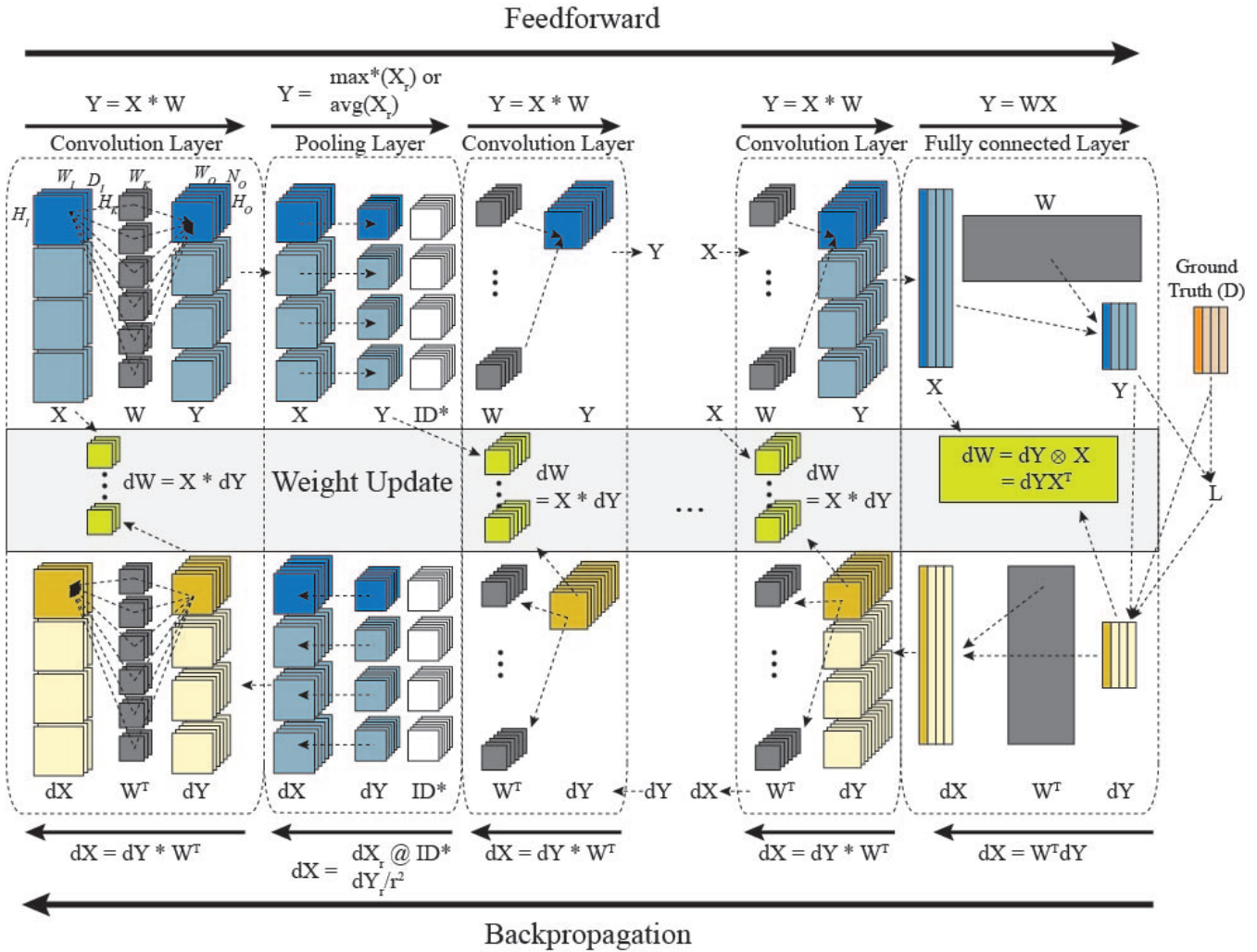


Figure 2: Deep neural network composed of convolution layer, pooling layer, and fully connected layer. It has three phases: feedforward, backpropagation, and weight update (ID*: location of maximum pixel in pooling area).

forward in convolution and fully connected layer except *transposing kernel* (Fig. 2).

2.3 Weight Updates (UP)

Based on dX , $\partial L / \partial W (dW)$ needs to be generated to reduce L in next iteration (epoch). New W for next iteration is determined as $W_{new} = W_{old} - \eta \cdot dW$, where η is learning rate. Recently, additional term is added during the update such as momentum [17]. For convolution, it needs convolution between X and dY . As dimension of dY is smaller than X by radius of kernel (W), it is convolution with very large kernel size. For fully connected layer, it requires vector vector outer product. Thus we can see there is *additional* operation and data flow is needed for efficient operation in weight updating.

2.4 Data Preparation (Prep)

For each operation, input data need to be pre-loaded

into the memory to improve data flow between memory and processing engines. If the layout of output generated in layer i does not match with required data layout for the layer $i + 1$, it needs to be re-arranged between multiple memory banks. In addition, for convolution, to make the size of the output same as the size of input, the input needs *dummy* zeros on its boundary.

2.5 Minibatch Training

Mini batch training involves updating weights after training small set (K) of training data. If total number of training data is N , it will iterate N/K times for one epoch. It is faster than training with large batch sizes and shows smoother convergence than training individual images. Moreover, it can reuse weights K times improving computing efficiency [14]. However, it requires more on-chip memory to store K temporal data.

The multiple mini-batches are trained in parallel us-

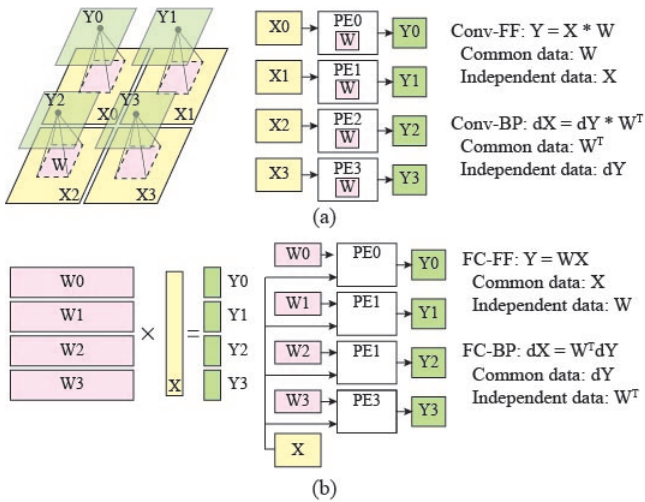


Figure 3: Hybrid Data Flow. (a) 2D convolution with small kernels and (b) Matrix multiplication

ing multiple computing nodes where each node independently compute $\partial L / \partial W (dW)$. After generating all dW s, all machine share updated new W (synchronous training) [18]. To overcome the unbalance in training latency among multiple nodes, in asynchronous training once a node generates dW , it will have new W while others use old W [19].

3. PROPOSED ARCHITECTURE

In this paper, NeuroTrainer is designed considering a Hybrid Memory Cube (HMC) where a 3D memory stack is partitioned into multiple parallel vaults. For example, HMC 1.0 is composed of 4 DRAM dies partitioned into 16 vaults, each vault has an independent memory controller (vault controller, VC), and connected to 4 external (off-chip) links via AXI interface. The computation fabric of NeuroTrainer is composed of multiple processing engines (PEs) where each PE contains clusters of computation units and local buffers for inputs (states) and parameters. Each PE has a one high bandwidth connection to its local vault and an interface to a broadcast bus connected to a shared vault. The vault controllers are augmented with a programmable memory address generator (PMAG), a state-machine that realizes mapping of the different types of data (input, parameter, and gradients) to different vaults and control data flow between memory and PEs.

3.1 Hybrid Data Flow

NeuroTrainer is designed to provide two different data movements between vaults and PEs based on the operation types. Consider convolution and matrix-matrix multiplication. During the convolution (Fig. 3 (a)), kernel (W) is shared by PEs while input is partitioned for each PE. For the matrix-matrix multiplication, weight matrix (W) is partitioned while input (X) is shared by PEs. We note that one of the inputs can be shared by

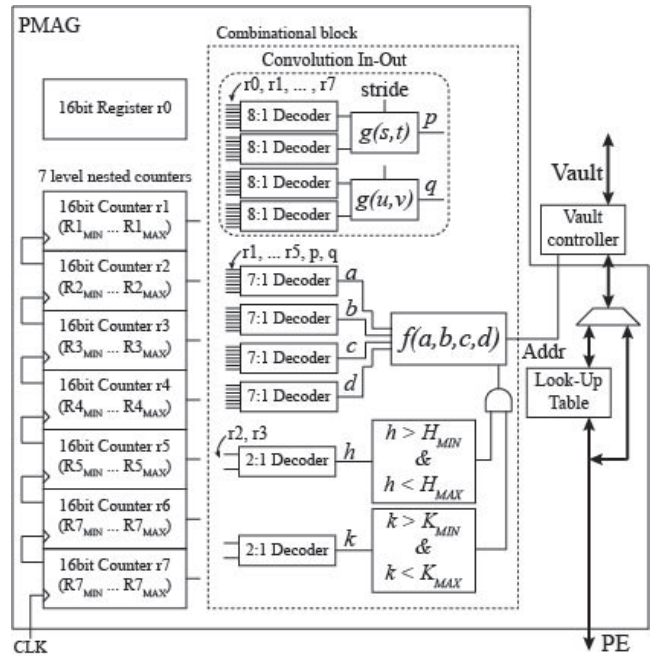


Figure 4: Block diagram of PMAG

all PEs in any operations of DNN.

Based on the size of common input, operations in Fig. 2 can be classified as *small common data* (ex: convolution with small kernels) and *large common data* (ex: matrix-matrix multiplication). For example, the weights of small kernels in the convolution layer would be small common kernels whereas the large weight matrix in a fully connected layer corresponds to large common data. The approach used in NeuroTrainer is to buffer copies of small common data across PEs and stream partitions of large data (e.g. inputs to a layer) from the local vault. Alternatively, with respect to large common weight matrices, they can be broadcast from a shared vault to all PEs, while partial weight matrices are stored across PEs. These two classes of data flows are illustrated in Fig. 3.

The *data rearranging* among vaults is required to dynamically change data flow from one type of layer to another. However, in a DNN, a set of convolution layers is followed by a set of fully connected layers; therefore rearrange is required only once in both feedforward and backpropagation.

3.2 Programmable Memory Address Generator (PMAG)

The programmable memory address generator (PMAG) controls the data flow by providing memory address to the vault controller for read and write, and pushing the data through the NeuroTrainer. The PMAG is composed of 7-level nested counters ($r_1 \dots r_7$), combinational logic to generate address, and decoders to assign counter values as input of combinational logic (Fig. 4). The PMAG also computes the non-linear func-

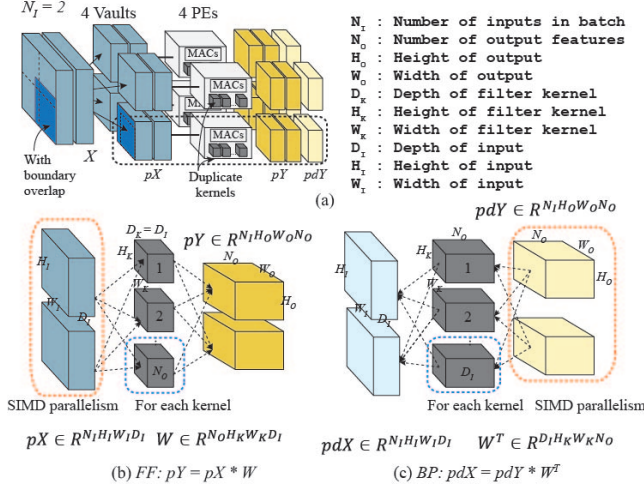


Figure 5: Convolution (X and W). (a) X is partitioned into 4 pX for 4 PEs, (b) Convolution feedforward, (c) Convolution backpropagation.

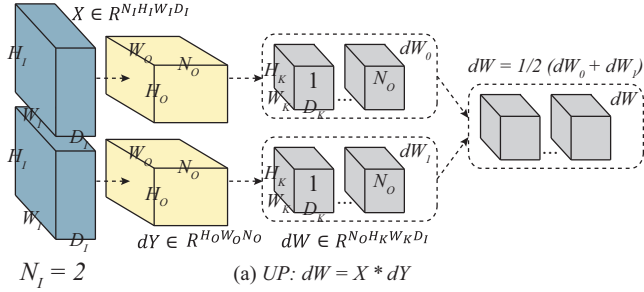


Figure 6: Convolution weight update when N_I is 2. It will generate dW_0 and dW_1 by $dW_i = X_i * dY_i$. Final dW is average of dW_0 and dW_1 .

tion (and its derivative) by using look up tables [LUTs, for $f(x)$ and $f'(x)$] for (a) activation function (ReLU, tanh, etc.) or (b) exponential/logarithm for softmax and cross-entropy layer.

Convolution Feedforward / Backpropagation.

Fig. 5 shows input X is partitioned into 4 pX with boundary overlap for convolution (assume 4 PEs). As kernel size is small, kernels are duplicated into all PE's buffers. For each kernel (outer most loop is N_O), N_{MAC} inputs are processed in parallel (SIMD). For backpropagation, transpose of W (W^T) is required and it can be handled in PE without reshaping data in the buffer of PE. It will be explained in Section 3.3.4.

Convolution Weight-update. After generating dY , dW is needed to update weights. Fig. 6 shows convolution weight update when N_I is 2. For each sample (X_i), $dW_i = X_i * dY_i$ is computed, and final dW is computed by averaging all dW_i s. Although weight update is also convolution between X and dY , the kernel size (W_O by H_O) is similar to the input size (W_I by H_I). Due to large kernel (dY), partitioning input (X) with bound-

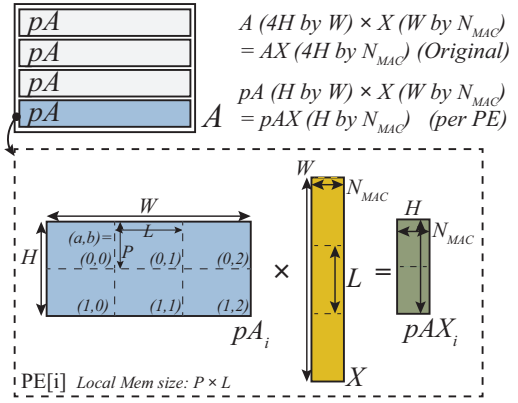


Figure 7: Matrix-matrix multiplication using 4 PEs. Each PE computes $pA \times X = pAX$.

ary overlap (Fig. 5) is inefficient and duplicating dY into all PEs is impractical. Therefore, we convert convolution with large kernel to matrix matrix multiplication by lowering convolution similar to how cuDNN performs convolution [20] (Fig. 6 (b)). Although drawback of lowering is increasing memory requirement from X_i to X_{M_i} , in-memory computation in NeuroTrainer can resolve the memory challenge.

Matrix-matrix multiplication. The main operation of fully connected layer or recurrent layer is matrix-matrix multiplication ($A \times X = AX$) [21, 22]. Fig. 7 shows that A is divided into 4 pA_i (i : PE index) row-wise and how a single pA_i is partitioned to small blocks (each size is $L \times P$), which is fitted into half size of buffer in PE (double buffering). As explained in Section 3.1, two data paths operate in matrix matrix multiplication (large common data) and the PMAG with common data vault and the PMAG with independent data vault are programmed separately. Fig. 7 shows that pA_i is partitioned into 3 by 2 blocks. After processing first 3 blocks of pA_i and X , a block of pAX_i is generated (size = N_{MAC} by H). The pAX_i needs to be delivered to common data vault.

Vector-Vector Outer product. For weight update in FC layer, for each sample in batch, input (X) and gradient (dY) need to be multiplied to generate dW . Contrast to matrix-matrix multiplication, N_i samples cannot be unlooped in SIMD level. In other words, this operation should be repeated N_i times and dW needs to be averaged. Fig. 8 shows vector-vector outer product using 4 PEs. Vector A is divided into 4 vaults (pA_i , size = H) and B will be stored in common data vault and will broadcast. The operation inside PE is similar to that of matrix matrix multiplication, however, the output ($pA_i pB^T$) does not need to be merged to common vault since it's gradient of weight in FC layer; therefore it's written back to dedicated vault.

Data Preparation Fig. 5 (a) shows that convolution with 4 PEs generates 4 pY s in parallel. If it is the last convolution layer before fully connected layer, the outputs of convolution layer should be **merged** into common data vault before to be broadcast in matrix

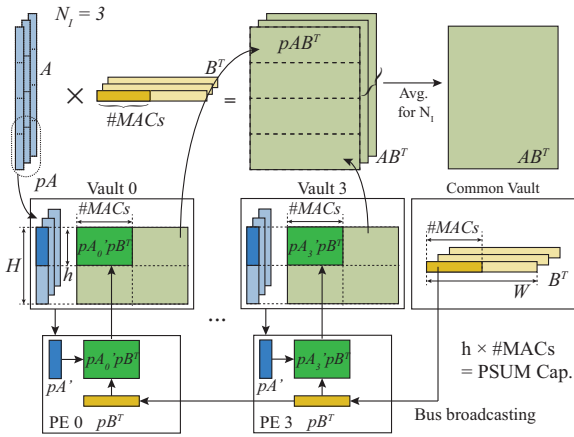


Figure 8: Vector-vector outer multiplication using 4 PEs. Each PE computes $pA \times B^T = pAB^T$.

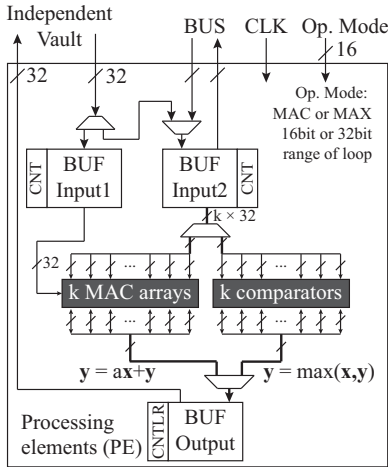


Figure 9: Block diagram of PE composed of three local buffers (input1, input2, and output), k MAC, k comparators.

matrix multiplication (Fig. 3). The order of PE to send data is pre-determined in the BUS. Based on this order, PMAG connected to common data vault also knows the portag in the merged data (PW , PH). In similar way, data from common data vault is also **partitioned** to all other vaults.

Add/remove zero boundary. Before convolution, input needs to be **zero padded** on the boundary to return same sized output based on the kernel radius r .

3.3 Processing Elements (PE)

A processing element is composed of a k MACs array, k comparators, and three local buffers: two input buffers, one output buffer (partial sum) (Fig. 9). Similar to PMAG, PE also needs to be programmed before the main computation.

3.3.1 Local Buffers

To avoid stall of PE (idle mode) due to lack of operands

Table 1: Comparison of different fixed point MAC designs with IEEE 754 single precision floating point MAC. All designs are synthesized with 15nm FinFet [23] operating 2.5GHz.

	Area (μm^2)	Power (mW)
Float 32	2093.88	5.37
Fixed 32/16	986.23 (-52%)	2.27 (-57%)
Fixed 32/16 SR [24]	2072.44 (+1%)	5.79 (+7%)
Fixed 32/16 SR LO	1578.71 (-24%)	3.78 (-30%)

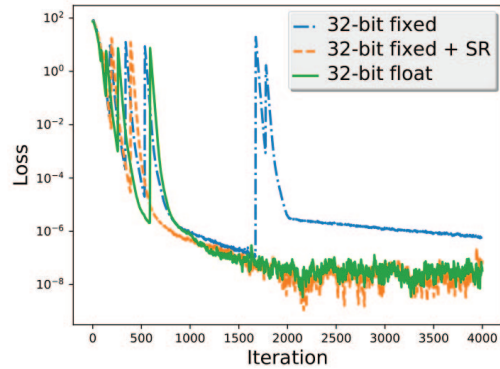


Figure 10: Training accuracy for RNN with different numeric representation (SR: Stochastic Rounding).

(inputs), we use two inputs and output buffers in PE. For each buffer, while half of memory is consumed by MACs (computing operation), rest of buffer can be filled simultaneously (double buffering). All local buffers have address generator based on nested counters. In Fig. 9, CNT2 is two level nested 16bit counters and CNT1 is single level 16bit counter. Data stream between DRAM and PE ends with END-MARK (0xFFFF for 16bit case, 0xFFFFFFFF for 32bit case) Computing in the PE starts only both input buffers are ready (half filled).

3.3.2 Multiply and Accumulate Units

As primitive arithmetic operator, a row of k multiplier and accumulator (MAC) units is placed in a PE. Although, reduced precision (16 bit fixed-point) is acceptable for inference (forward propagation), even 32bit fixed point in backpropagation and parameter update may result in inaccurate training in deeper network, in particular, the recurrent networks [25] as illustrated in Fig. 10. We should note that there is no accuracy degradation between SR and SR LO. The stochastic rounding (SR) can be applied to overcome *quantization* error in fixed point [26, 25].

Therefore, we design MAC to operate 1) two pairs of 16bit operands or 2) a pair of 32bit operands (Fixed 32/16). To add stochastic rounding, 64 random number generators are added [25] (Fixed 32/16 + SR). To reduce power/area overhead, we propose to add a single random number generator is used and it generates a single bit in every clock (**Fixed 32/16 + SR LO**,

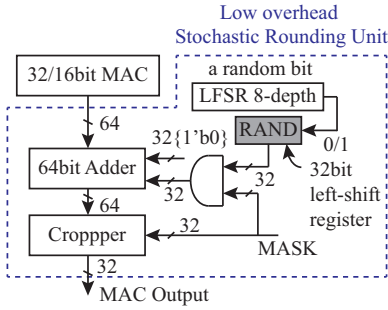


Figure 11: Fixed 32/16 + SR LO: Fixed 32/16bit MAC with low overhead stochastic rounding unit: a single LFSR and 32bit left shift register.

Fig. 11)). Synthesis in 15nm FinFET [23] shows that proposed design provides higher energy-efficiency (Table 1) while providing similar training accuracy as floating point design. The MAC operates in the 16bit mode without SR during inference (forward propagation).

3.3.3 Comparator Unit

Since MAX operation is required only for the max-pooling inference, 16 bit fixed point comparators are placed in PE. Based on pooling radius (r), r^2 data are streamed into controller, and the comparator unit returns the maximum value and its ID for backpropagation.

3.3.4 PE Operation

After two input buffers are filled (BUF Input 1 and BUF Input 2), BUF Input 1 pushes one 32bit input (one 32 bit operand or two 16 bit operands) while BUF Input 2 pushes k (N_{MAC}) 32bit inputs. For MAC operation (all cases except max pooling), k MAC arrays compute $\mathbf{y} = \mathbf{ax} + \mathbf{y}$, where \mathbf{x} and \mathbf{y} are vectors, which length is k (32bit) or $2k$ (16bit). For MAX operation (max pooling), k comparator returns max value as $\mathbf{y} = \max(\mathbf{x}, \mathbf{y})$.

Convolution. In convolution, k inputs are processed by k MACs in parallel (SIMD level). Therefore, kernels are stored in BUF Input 1 and k inputs are stored in BUF Input 2. If k inputs cannot be stored in BUF Input 2 due to capacity issue, k subsets of k inputs are stored and newly required input ($k \times H_k$) is updated during the operation similar to [3]. For convolution backpropagation, W^T is easily obtained by sweeping counter values in CNT2 attached to BUF Input 1.

Matrix-Matrix multiplication. Similar to convolution, k inputs are processed in parallel (SIMD level). Therefore, partial weight matrix is loaded in BUF Input 1 and k partial inputs are stored in BUF Input 2. After consuming one partial weight matrix [a,b] (P by L in Fig. 7), next partial weight matrix [a,b+1] is processed. Similar to convolution, W^T is obtained by sweeping counter values in CNT2 attached to BUF Input 1.

Vector-Vector outer product. In fully connected update, k inputs cannot be processed in parallel. In

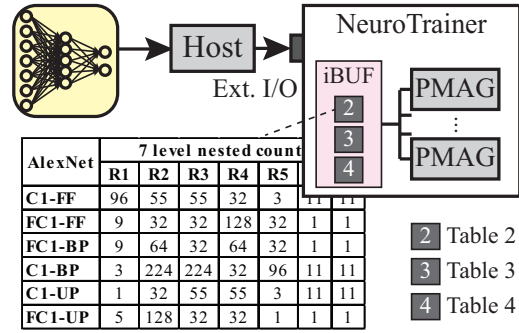


Figure 12: Programming NeuroTrainer by host for given DNN.

computing AB^T , A is loaded in BUF Input 1 and B is loaded in BUF Input 2. In other words, k elements of B is delivered into k MAC units in a single clock (Fig. 8).

3.4 BUS Interface

Bus interface has two operation modes controlled by common data vault: broadcasting to all PEs and merging data into common data vault from all PEs. The BUS and PE communicates using three-way handshaking (REQ-ACK-SEND) for both operations. Broadcasting mode is set when all PE can take data (input buffer is ready) and during the broadcasting, any REQ from PE is ignored (broadcasting is prior to merging mode). During the merging mode, all PE send REQ and get ACK from the bus based on predetermined priorities among PEs. Although all 15 PEs request BUS for writing-back simultaneously, the impact of latency of entire writing back (for 15 PEs) on the throughput can be minimized as PE's computing latency dominates entire computing latency. The bus architecture is designed and synthesized to guarantee a bandwidth same as that of a single vault (10GBps). We use 4 stage pipelined BUS interface [27]; it takes 4 clock cycle between a vault to any PE.

4. PROGRAMMING

Following the discussions in Section 3.2, Table 2 and Table 3 summarize the PMAG programming which includes setting range of 7 nested loops ($r1 \sim r7$) and connecting counter values to combination logic for different operations. For matrix-matrix multiplication (FC-FF/BP) and vector outer product (FC-UP), C.Vault is the programming value for PMAG attached to common data vault and I.Vault is the programming value for PMAG attached to independent data vault. Similar to PMAG, PE needs to be programmed to set: 1) operation type: MAC or MAX, 2) bit precision mode for MAC: 16 bit or 32 bit with/without SR, and 3) loop range for address generator for local buffers. Based on the discussions in Section 3.3.4, Table 4 summarizes the inputs for PE programming for different operations. In essence, the preceding three tables defines the instruction set architecture of the NeuroTrainer.

Given a DNN, the host first generates the preced-

Table 2: Programming PMAG for Convolution and Fully connected layer

	7 level nested counters							Conv. In - Out				f (a,b,c,d)			
	R1	R2	R3	R4	R5	R6	R7	p		q		a	b	c	d
								s	t	u	v				
Conv-FF	N_O	H_O	W_O	N_I	D_K	H_K	W_K	r2	r6	r3	r7	r4	q	p	r5
Conv-BP	D_I	H_I	W_I	N_I	N_O	H_K	W_K	r2	r6	r3	r7	r4	q	p	r5
Conv-UP	1	N_I	H_O	W_O	D_I	H_K	W_K	r3	r6	r4	r7	q	p	r5	r2
FC-FF/BP (C. Vault)	H/P	W/L	P	L	K	1	1	-	-	-	-	r4	r2	r5	0
FC-FF/BP (I. vault)	H/P	W/L	P	L	K	1	1	-	-	-	-	r4	r3	r2	r1
FC-UP (C vault)	H/h	$\frac{W}{N_{MAC}}$	N_I	N_{MAC}	1	1	1	-	-	-	-	r4	r3	r2	r1
FC-UP (I. vault)	H/h	$\frac{W}{N_{MAC}}$	N_I	h	1	1	1	-	-	-	-	r4	r3	r2	r1

a, b, c, d, p, q, s, t, u, and v are labels used in Fig. 4.
R1 ~ R7: maximum value of r1 ~ r7 loop. (minimum value are all zero)

Table 3: Programming PMAG for data rearranging and data preparation

	7 level nested counters			Conv. In - Out				f (a,b,c,d)				Two comparators			
	R1	R2	R3	p		q		a	b	c	d	h	H	k	K
				s	t	u	v								
Merge	D_I	PH_I	PW_I	-	-	-	-	r3	r2	r1	0	-	-	-	-
Partition	D_I	H_I	W_I	-	-	-	-	0	0	0	1	r2	$0 \sim PH_I$	r3	$0 \sim PW_I$
Add pad	D_I	PH_I	PW_I	r3	r	r2	r	p	q	r1	0	r3	$r \sim r + W_I$	r2	$r \sim r + H_I$
Remove pad	D_I	PH_I	PW_I	-	-	-	-	r3	r2	r1	0	r3	$r \sim r + W_I$	r2	$r \sim r + H_I$

a, b, c, d, p, q, s, t, u, and v are labels used in Fig. 4.
R1 ~ R3: maximum value of r1 ~ r3 loop. (minimum value are all zero)
R4 ~ R7: 1

Table 4: PE Program for computing operations

	Bit	CNT2	CNT1
Conv-FF	16	H_K, W_K	$W_K \times H_K$
Conv-BP	32	H_K, W_K	$W_K \times H_K$
Conv-UP	32	P, L	L
FC-FF	16	P, L	L
FC-BP	32	P, L	L
FC-UP	32	h	1

H_K, W_K : dimension of convolution kernels
 P, L : dimension of partial matrix (Fig. 7)
h: length of partial vector (Fig. 8)

ing three tables. Fig. 12 illustrates the programming process of the NeuroTrainer. To enable *autonomous operation* of the NeuroTrainer, we embed an on-chip instruction buffer (iBuffer) to store the preceding three tables (Figure 1(a)). Given a DNN, the host generates the preceding three tables and loads them in the iBuffer. During execution the layer-wise operation is

controlled by the iBuffer (using a layer counter). To estimate the size of the iBuffer, consider that for a network with N layers, we need to program NeuroTrainer $\sim 4N$ times (Feedforward, backpropagation, weight update, data preparation if needed). Each time the amount of data for programming is 22Byte (18Byte for PMAG and 4Byte for PE). Therefore, a 16KB memory is sufficient as iBuffer and it can cover 186 layers. The latency of programming the iBuffer through HMC external interface is negligible compared to loading the input data.

5. SIMULATION RESULTS

5.1 Performance Analysis

The performance of the NeuroTrainer is simulated using cycle-level simulator. All simulation results is based on minibatch size 32, which is recommended minimum size of minibatch [28]. All MACs, comparators, buffer in PE, BUS interface, PMAG are synthesized operate at 2.5GHz to maximize the single vault's bandwidth.

Fig. 13 shows throughput (TOPS/s) and latency (sec-

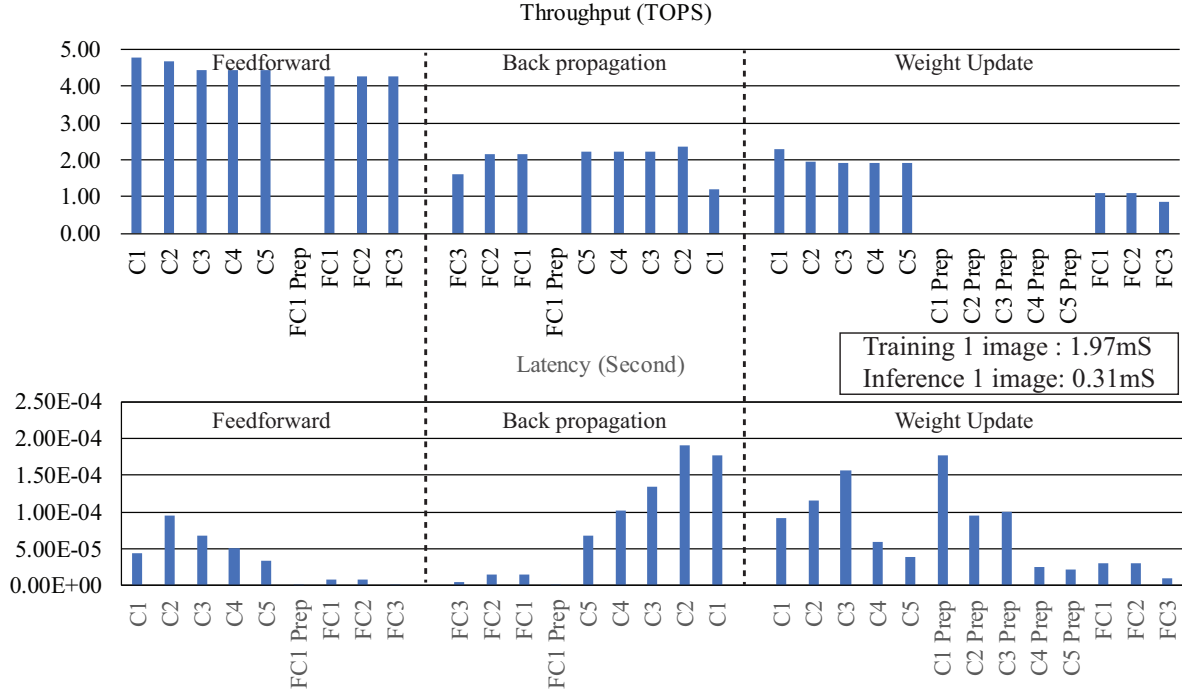


Figure 13: Simulation result for Alexnet in terms of latency (second) and throughput (Tera-Ops/sec: TOPS/s). C1 - C5: convolution layer, FC1 - FC3: fully connected layer, Prep: data preparation

ond) for a single input of each layer in Alexnet. For the one input image, inference took 0.31mS (3,228 images per second) and training took 1.97mS (507 images per second).

In feedforward phase, all convolution or fully connected layers shows similar throughput above 4.0 TOPS/s (4.2TOPS/s \sim 4.7TOPS/s) which is close to the theoretical maximum for 16bit operation of our MAC ($2.5\text{GHz} \times 15 \text{ PEs} \times 32 \text{ MACs} \times 2 \text{ pairs inputs} \times 2$ (multiplication and addition) = 4.8TOPS/s).

For backpropagation and weight update, 32bit with stochastic rounding is used. Theoretical maximum throughput can be computed as 2.4 TOPS/s in the same manner. In backpropagation, FC3 (1.61 TOPS/s) and C1 layer (1.19 TOPS/s) show lower throughput than others. For FC3 backpropagation, the size of dY is not large enough to hide latency of *writing back* from all PEs to a single vault. In other words, the latency to generate output by iterating dY times is shorter than writing back the output to common data vault; writing back becomes bottleneck in the system. For C1 layer, input dimension is $55 \times 55 \times 96$ and kernel dimension is $11 \times 11 \times 3$. It can be processed as convolution since kernel size is small enough to fit in the local memory; but efficiently due to large kernel size compared to input.

In weight update, C1 \sim C5 shows about 1.98 TOPS/s by translating convolution as matrix multiplication in large kernel case. However, FC layer (vector vector outer multiplication) shows about 1.02 TOPS/s, which is the worst case due to high network traffic between PE and independent vault since there is no data re-usage.

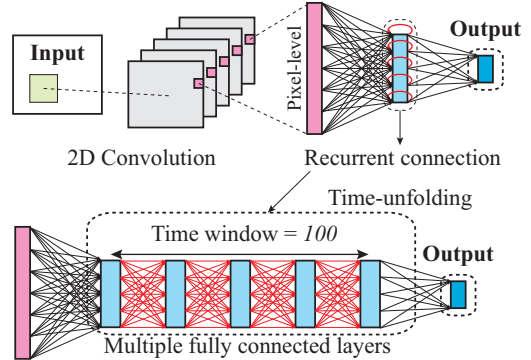


Figure 14: Simplified example of DNN for generating sentences for image description [29].

To see the performance of more complex and deeper network, we evaluate a DNN for generating image description [29], image feature extraction part is implemented as Alexnet and RNN (GRU) is attached after 5th convolution layer (Fig. 14). A single GRU is composed of six fully connected layers for hidden neurons and one fully connected layer for output neurons. The number of input neurons in GRU is 43,264 and the number of hidden neurons in GRU is 10,000. We assume T for DNN is 100. Fig. 15 shows latency of each layer in DNN explained earlier. For the recurrent layers (in the dashed box), the latency is computed considering time windows (latency to across all time unfolded T layers); that's why it shows high latency than other layers.

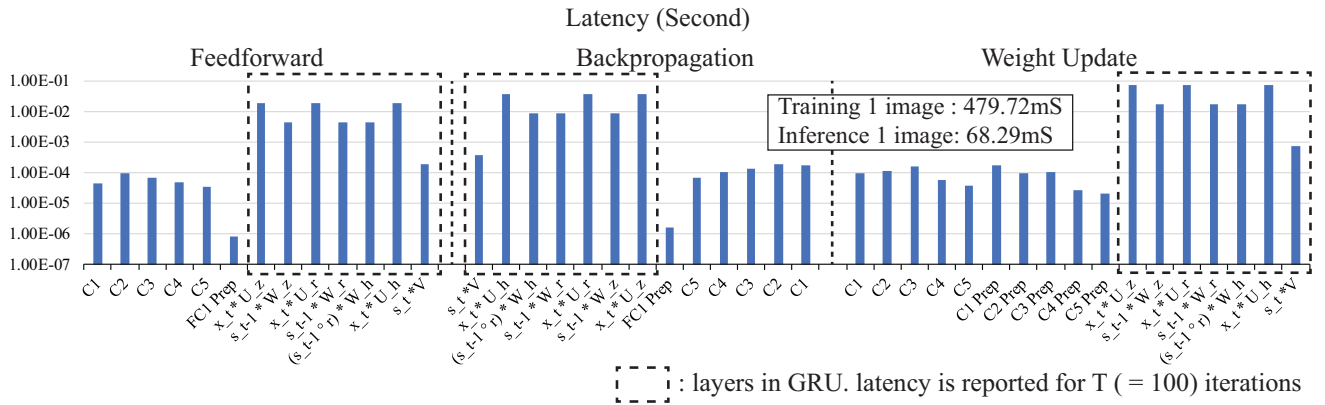


Figure 15: Latency analysis of each layer in DNN [29].

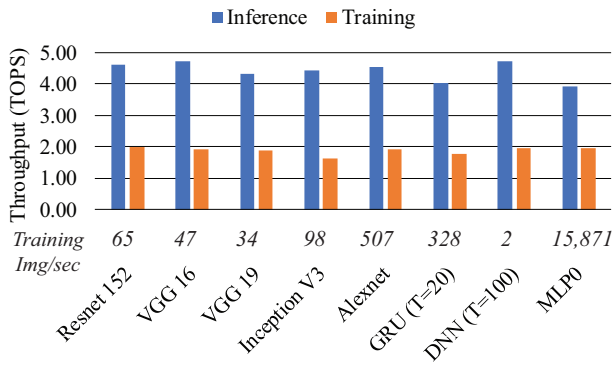


Figure 16: Simulation results for different benchmarks.

Fig. 16 shows the throughput for various benchmarks including Resnet 152 [30], VGG 16, VGG 19 [31], Inception V3 [32], GRU [22], DNN for image description [29], and MLP0 [9] are also tested. Y-axis represent the throughput (TOPS/s) and the number on the X-axis represent the number of inputs that can be trained in a second for each benchmark. For all benchmarks, inference shows 4.0 ~ 4.7 TOPS/s and training shows 1.9 TOPS/s. Further, NeuroTrainer shows stable throughput (standard deviations less than 6% of average) for training with all benchmarks of varying complexity.

5.2 Synthesis and Power Analysis

The computation fabric of the NeuroTrainer, including the PEs, bus interface, and PMAG with the vault controller is synthesized using 15nm FinFet [23]. As vault controller is a proprietary design, a 32bit SDRAM controller [27] is adopted as a reference vault controller. Table 5 summarizes average power across 8 different benchmarks and area overhead of each module in the system. Total power consumption of logic layer is 2.64W and area overhead (including vault controller) is 1.17mm². Even scaled up to compare with previous result syn-

Table 5: Power and Area analysis of NeuroTrainer synthesized in 15nm FinFet [23].

	Area (mm ²)	Power (W)
PE	6.96E-02	1.55E-01
PMAG	2.00E-03	3.16E-03
Vault Ctrl.	7.73E-04	4.27E-03
32bit Bus	8.96E-03	3.70E-02
16KB: I-BUF	5.51E-03	1.02E-02
Logic die	1.17E+00	2.65E+00
4 DRAM dies		2.03E+00

thesized in 28nm CMOS [33], total area is less than 5% of footprint of fabricated HMC (68mm²). Average DRAM die power is computed during the simulation using 3.7pJ/bit from [33] and actual DRAM access pattern. The power densities of the logic die (0.039W/mm²) and DRAM dies (0.030W/mm²) in NeuroTrainer is well within the acceptable power densities (1.5W/mm², [34], of 3D stacked systems.

From DRAM power consumption (2.03W), average memory bandwidth can be computed as 68.5GByte/sec (2.03W/3.7pJ/bit), which is lower than total aggregated memory bandwidth of HMC (16 vaults × 10GByte/sec). With batch size of 32, weights are reused 32 times. DRAM utilization can be increased by, 1) more MACs per PE, but requires larger partial sum SRAM and less efficient for the small batch (minimum batch size for most of DLs is 32) and 2) more PEs, but it requires a larger network among PEs and vaults.

On average, NeuroTrainer consumes 4.64W and delivers 1.89 TFLOPS throughput and 406 GFLOPS/W of efficiency during training (32bit) while maintaining high training accuracy.

For HMC 2.0 [35], performance is estimated (Table 6). With 32 vaults, 31 PEs can be placed; therefore throughput and logic power increases about twice. However, power of DRAM dies is same since total memory access is constant. Therefore, it shows 39% gain in efficiency.

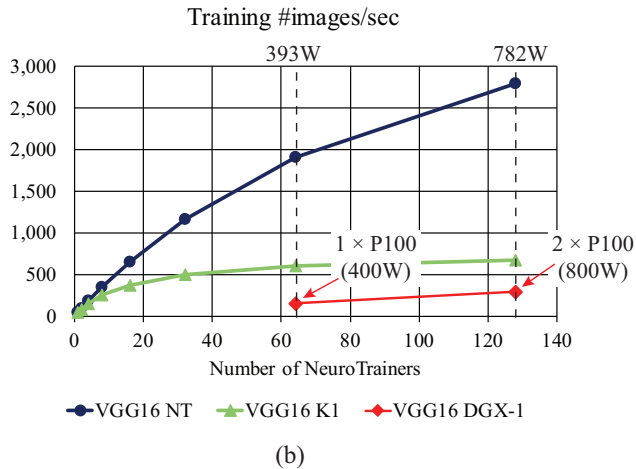
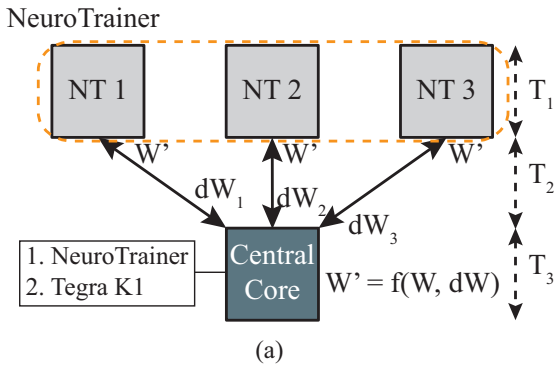


Figure 17: Scalability: (a) system of multiple NeuroTrainer. (b) Performance for VGG16 with central core being NeuroTrainer (VGG16 NT), Tegra K1 (VGG16 K1), and DGX-1 (P100) (VGG16 DGX-1).

5.3 Scalability to Multiple NeuroTrainers

The multiple NeuroTrainer can be used in parallel for scalable training performance as illustrated in Fig. 17 (a). As all NeuroTrainer take same latency (T_1) for training a minibatch, we propose to perform **synchronous** training [18]. After training a single input batch, N NeuroTrainer delivers dW to a central unit (latency = T_2). The central unit needs to take all dW from N NeuroTrainer s, and generates new W (W') following: $W' = \eta \times average(dW) + W$, where η is learning rate. The above computation can be performed by another NeuroTrainer. However, to cover more generic approaches for weight update (e.g. AdaGrad [36] or Adam [37]), a software implementation, for example, using Tegra K1 (326 GFLOPS, 10W, 28nm) [38] can also be considered.

Fig. 17 (b) shows estimated training performance (number of images per second) of VGG 16 [31] by different number of NeuroTrainers and two different types of central core. Training performance using high-end GPU (NVIDIA DGX-1) is also reported. This estimated performance is computed based on peak FLOPS of each

Table 6: Comparison with previous training accelerators

Work	NC [4]	NS [6]	SD [13]	NT
Bit	16 FI	32 FL	16 FL /32FL	16 FI /32 FI*
Node (nm)	15	28	14	15
Peak TFLOPS	0.13	0.96	1400 /680	4.4(9.6) /1.9(4.1)
Power (W)	3.4	42.8	1,400	4.7(7.2)
Efficiency	38.8	22.5	331.7	406(566)

NC: NeuroCube, NS: NeuroStream, SD: ScaleDeep, NT: NeuroTrainer.

FL: floating point, FI: fixed point, FI*: fixed point with stochastic rounding

Efficiency: $GFLOPS/W$

For NT, () indicates *estimated* for HMC 2.0
For NT, power is averaged across 8 benchmarks illustrated in Fig. 16.

processing unit and HMC external BW. For example, Tegra K1 (326 GFLOPS) can update weights in 42.4mS for AlexNet (138M parameters) since itãŽs element-wise operation. The latency between a NeuroTrainer and K1 is 4.61mS (240 GByte/sec). If system is composed of 4 NeuroTrainers with a K1 as host, total latency is 63.1mS (training latency in NeuroTrainer) + 42.4mS \times 4 (K1 needs update W using 4 dW s) + 2 \times 4 \times 4.61mS (round trip from a K1 to 4 NeuroTrainers) = 269.58mS while training 4 \times 32 samples. In the same manner, a single P100 in DGX-1 can train 150 images per second [39] with 400W power consumption. For the same power budget, 64 NeuroTrainer can operate in parallel and train 1,900 images delivering 13x speedup. The additional power consumption due to off-chip data movement estimated using HMC access energy of 10pJ/bit [33]. Ultimately, the performance scaling in NeuroTrainer is limited by the off-chip latency showing need for better system architecture and faster off-chip network.

6. RELATED WORK

Table 6 compare NeuroTrainer with previously reported DNN training accelerators. NeuroCube [4] and NeuroStream [6] presents inference engines using in-memory accelerators, which can also perform training. The results demonstrate higher efficiency over a GPU-baseline showing the promise of hardware acceleration. However, performance gain is nominal as no hardware was optimized for training.

Scaledeep [13] proposes specialized hardware for different computation kernels. A multi-chip module is synthesized using five different tiles (heterogeneous architecture) and allocating layers to different tiles based on their property (such as Byte/Ops). The design demonstrates better power efficiency over GPUs.

The main difference between NeuroTrainer and ScaleDeep is the orthogonal approaches to optimize efficiencies of different kernel. Rather than changing a data flow in the hardware for different operations as performed in NeuroTrainer, ScaleDeep decides the tile distribution during design. Consequently, if the layer distribution in DNN architecture does not match the tile distributions, for example, if one kind of layer (convolution or fully connected) dominates the entire network, the tile utilization and efficiency is low. This effect is evident from [13] (see Fig. 20) which shows even for various CNN benchmarks, the standard deviation of efficiency is about 28% of average, which is expected to increase further if recurrent networks are considered.

In contrast, the NeuroTrainer uses a homogeneous architecture and dynamically changes the data flow and data mapping to optimize the performance of individual layers. The dynamic optimization, instead of design time decisions, allow NeuroTrainer to maintain similar throughput for much wider classes of benchmarks even including RNNs. The homogeneous architecture also makes the design easier to scale for parallel training. The secondary difference comes from the use of 3D in-memory acceleration in NeuroTrainer to reduce data movement power, and fixed point arithmetic with stochastic rounding for higher efficiency (compared to floating point in ScaleDeep).

7. CONCLUSION

We have presented NeuroTrainer, an intelligent memory module with in-memory accelerators for energy-efficient training of different classes of DNNs. The NeuroTrainer utilizes a programmable data flow based execution model to optimize memory mapping and data reuse during different phases of training operation. The simulation results demonstrate potential for appreciable performance and power-efficiency gain over baseline GPU or alternative accelerators. The NeuroTrainer can form the building block of a scalable architecture for energy efficient training for deep neural networks. Ultimately, the performance scaling in a scalable training platform with NeuroTrainer is limited by the off-chip latency showing need for future research on better system architecture and faster off-chip network.

8. REFERENCES

- [1] S. Han, X. Liu, H. Mao, *et al.*, “Eie: efficient inference engine on compressed deep neural network,” *arXiv preprint arXiv:1602.01528*, 2016.
- [2] Y. Chen, T. Luo, S. Liu, S. Zhang, L. He, J. Wang, L. Li, T. Chen, Z. Xu, N. Sun, *et al.*, “Dadiannao: A machine-learning supercomputer,” in *Microarchitecture (MICRO), 2014 47th Annual IEEE/ACM International Symposium on*, pp. 609–622, IEEE, 2014.
- [3] Y.-H. Chen, J. Emer, and V. Sze, “Eyeriss: A spatial architecture for energy-efficient dataflow for convolutional neural networks,” in *Computer Architecture (ISCA), 2016 ACM/IEEE 43rd Annual International Symposium on*, pp. 367–379, IEEE, 2016.
- [4] D. Kim, J. Kung, S. Chai, *et al.*, “Neurocube: a programmable digital neuromorphic architecture with high-density 3d memory,” in *Computer Architecture (ISCA), 2016 ACM/IEEE 43rd Annual International Symposium on*, pp. 380–392, IEEE, 2016.
- [5] M. Gao, J. Pu, X. Yang, *et al.*, “Tetris: Scalable and efficient neural network acceleration with 3d memory,” in *Proceedings of the Twenty-Second International Conference on Architectural Support for Programming Languages and Operating Systems*, pp. 751–764, ACM, 2017.
- [6] E. Azarkhish, D. Rossi, I. Loi, *et al.*, “Neurostream: Scalable and energy efficient deep learning with smart memory cubes,” *arXiv preprint arXiv:1701.06420*, 2017.
- [7] E. Nurvitadhi, J. Sim, D. Sheffield, *et al.*, “Accelerating recurrent neural networks in analytics servers: Comparison of fpga, cpu, gpu, and ASIC,” in *Field Programmable Logic and Applications (FPL), 2016 26th International Conference on*, pp. 1–4, EPFL, 2016.
- [8] D. Shin, J. Lee, J. Lee, and H.-J. Yoo, “14.2 dnu: An 8.1 tops/w reconfigurable cnn-rnn processor for general-purpose deep neural networks,” in *Solid-State Circuits Conference (ISSCC), 2017 IEEE International*, pp. 240–241, IEEE, 2017.
- [9] N. P. Jouppi, C. Young, N. Patil, *et al.*, “In-datacenter performance analysis of a tensor processing unit,” in *Proceedings of the 44th International Symposium on Computer Architecture*, IEEE Press, 2017.
- [10] <https://www.tensorflow.org/performance/benchmarks/>.
- [11] S. Hochreiter, “Untersuchungen zu dynamischen neuronalen netzen,” *Diploma, Technische Universität München*, p. 91, 1991.
- [12] S. Hochreiter, Y. Bengio, P. Frasconi, *et al.*, “Gradient flow in recurrent nets: the difficulty of learning long-term dependencies,” 2001.
- [13] S. Venkataramani, A. Ranjan, S. Banerjee, D. Das, S. Avancha, A. Jagannathan, A. Durg, D. Nagaraj, B. Kaul, P. Dubey, *et al.*, “Scaleddeep: A scalable compute architecture for learning and evaluating deep networks,” in *Proceedings of the 44th Annual International Symposium on Computer Architecture*, pp. 13–26, ACM, 2017.
- [14] S. S. Haykin, S. S. Haykin, S. S. Haykin, and S. S. Haykin, *Neural networks and learning machines*, vol. 3. Pearson Education Upper Saddle River, 2009.
- [15] J. L. Elman, “Finding structure in time,” *Cognitive science*, vol. 14, no. 2, pp. 179–211, 1990.
- [16] R. A. Dunne and N. A. Campbell, “On the pairing of the softmax activation and cross-entropy penalty functions and the derivation of the softmax activation function,” in *Proc. 8th Aust. Conf. on the Neural Networks, Melbourne, 181*, vol. 185, 1997.
- [17] N. Qian, “On the momentum term in gradient descent learning algorithms,” *Neural networks*, vol. 12, no. 1, pp. 145–151, 1999.
- [18] F. N. Iandola, M. W. Moskewicz, K. Ashraf, and K. Keutzer, “Firecaffe: near-linear acceleration of deep neural network training on compute clusters,” in *Proceedings of the IEEE Conference on Computer Vision and Pattern Recognition*, pp. 2592–2600, 2016.
- [19] J. Dean, G. Corrado, R. Monga, K. Chen, M. Devin, M. Mao, A. Senior, P. Tucker, K. Yang, Q. V. Le, *et al.*, “Large scale distributed deep networks,” in *Advances in neural information processing systems*, pp. 1223–1231, 2012.
- [20] S. Chetlur, C. Woolley, P. Vandermersch, J. Cohen, J. Tran, B. Catanzaro, and E. Shelhamer, “cudnn: Efficient primitives for deep learning,” *arXiv preprint arXiv:1410.0759*, 2014.
- [21] S. Hochreiter and J. Schmidhuber, “Long short-term memory,” *Neural computation*, vol. 9, no. 8, pp. 1735–1780, 1997.
- [22] J. Chung, C. Gulcehre, K. Cho, *et al.*, “Empirical evaluation of gated recurrent neural networks on sequence modeling,” *arXiv preprint arXiv:1412.3555*, 2014.
- [23] “Nangate FreePDK15 Open Cell Library.” http://www.nangate.com/?page_id=2328.
- [24] T. J. Chainer, M. D. Schultz, P. R. Parida, and M. A. Gaynes, “Improving data center energy efficiency with advanced thermal management,” *IEEE Transactions on Components, Packaging and Manufacturing Technology*, 2017.
- [25] T. Na, J. H. Ko, J. Kung, and S. Mukhopadhyay, “On-chip training of recurrent neural networks with limited numerical precision,” in *Neural Networks (IJCNN), 2017 International Joint Conference on*, pp. 3716–3723, IEEE, 2017.
- [26] S. Gupta, A. Agrawal, K. Gopalakrishnan, and P. Narayanan, “Deep learning with limited numerical precision,” in *Proceedings of the 32nd International Conference on Machine Learning (ICML-15)*, pp. 1737–1746, 2015.
- [27] “OpenCores.” <http://http://opencores.org/>.
- [28] http://svail.github.io/rnn_perf/.
- [29] A. Karpathy and L. Fei-Fei, “Deep visual-semantic alignments for generating image descriptions,” in *Proceedings of the IEEE Conference on Computer Vision and Pattern Recognition*, pp. 3128–3137, 2015.
- [30] K. He, X. Zhang, S. Ren, and J. Sun, “Deep residual learning for image recognition,” in *Proceedings of the IEEE conference on computer vision and pattern recognition*, pp. 770–778, 2016.
- [31] K. Simonyan and A. Zisserman, “Very deep convolutional networks for large-scale image recognition,” *arXiv preprint arXiv:1409.1556*, 2014.
- [32] C. Szegedy, V. Vanhoucke, S. Ioffe, J. Shlens, and Z. Wojna, “Rethinking the inception architecture for computer vision,” in *Proceedings of the IEEE Conference on Computer Vision and Pattern Recognition*, pp. 2818–2826, 2016.
- [33] J. Jeddeloh and B. Keeth, “Hybrid memory cube new dram architecture increases density and performance,” in *2012 Symposium on VLSI Technology (VLSIT)*, 2012.
- [34] W. Huang, M. R. Stan, S. Gurumurthi, *et al.*, “Interaction of scaling trends in processor architecture and cooling,” in *Semiconductor Thermal Measurement and Management Symposium, 2010. SEMI-THERM 2010. 26th Annual IEEE*, pp. 198–204, IEEE, 2010.
- [35] Hybrid Memory Cube Consortium, “Hybrid memory cube specification 2.0,” 2014.
- [36] J. Duchi, E. Hazan, and Y. Singer, “Adaptive subgradient methods for online learning and stochastic optimization,” *Journal of Machine Learning Research*, vol. 12, no. Jul, pp. 2121–2159, 2011.
- [37] D. Kingma and J. Ba, “Adam: A method for stochastic optimization,” *arXiv preprint arXiv:1412.6980*, 2014.
- [38] T. NVIDIA, “K1: A new era in mobile computing,” *Nvidia, Corp., White Paper*, 2014.
- [39] <http://dlbench.comp.hkbu.edu.hk/>.